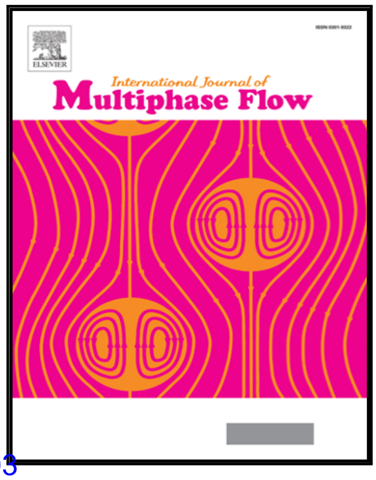

A novel model for the lift force acting on a prolate spheroidal particle in arbitrary non-uniform flow. Part II. Lift force taking into account the non-streamwise flow shear

Yan Cui, Jure Ravnik, Ožbej Verhnjak, Matjaž Hriberšek, Paul Steinmann

PII: S0301-9322(18)30313-6
DOI: https://doi.org/10.1016/j.ijmultiphaseflow.2018.12.003
Reference: IJMF 2936

To appear in: *International Journal of Multiphase Flow*

Received date: 25 April 2018
Revised date: 3 December 2018
Accepted date: 3 December 2018

Highlights

- A new generic method for the computation of the Saffman-type lift forces acting on a rigid particle in arbitrary non-uniform flows is presented.
- The method computes the shear-induced lift force taking into account also non-streamwise flow shear.
- A novel shear-induced lift force model is developed for prolate spheroidal particles by using this method.
- The accuracy and reliability of the proposed shear-induced lift model are verified and validated in Poiseuille and lid-driven cavity flows by comparing it with other Saffman-type lift force models.

A novel model for the lift force acting on a prolate spheroidal particle in arbitrary non-uniform flow. Part II. Lift force taking into account the non-streamwise flow shear

Yan Cui[a,*], Jure Ravnik[b], Ožbej Verhnjak[b], Matjaž Hriberšek[b], Paul Steinmann[a]

[a] *Chair of Applied Mechanics, Friedrich-Alexander Universität Erlangen-Nürnberg, Paul-Gordan-Str. 3, D-91052 Erlangen, Germany*
[b] *Faculty of Mechanical Engineering, University of Maribor, Smetanova 17, SI-2000, Maribor, Slovenia*

Abstract

The present contribution is the second part of a two-part research work presenting a generic method to extend lift force models that were originally devised for single linear shear flow to arbitrary flow conditions. The method can be applied to the computation of lift forces exerted on prolate spheroidal particles (or fibres) in arbitrary non-uniform flows. The method proposed in the Part I calculates the lift force arising from the dominant streamwise flow shear. In Part II the influence of the non-streamwise flow shear on the lift force is also taken into account. The present method assumes that the particle slip velocity is parallel to the fluid velocity along the particle trajectory. The novelty in the presented method is the computation of the shear lift force model for prolate spheroidal particles taking into account also non-streamwise flow shear. The accuracy of the novel shear lift force model for prolate spheroidal particles is verified by comparing it with the lift force model proposed in Part I via simulating the axial migration of a prolate spheroidal particle in the Poiseuille flow. In order to validate the ability of the present method for capturing the lift component

*Corresponding author
Email addresses: yan.cui@fau.de (Yan Cui), jure.ravnik@um.si (Jure Ravnik), ozbej.verhnjak@um.si (Ožbej Verhnjak), matjaz.hribersek@um.si (Matjaž Hriberšek), paul.steinmann@fau.de (Paul Steinmann)

arising from non-streamwise flow shear, the lift force model is compared with established generalised Saffman-type lift models by simulating the motion of a particle in lid-driven cavity flow. The computational results demonstrate that the present lift force model for prolate spheroidal particles is applicable in flow cases with streamwise and non-streamwise flow shear, even if some (reasonably small) accuracy for the case of the streamwise-only shear is lost.

Keywords: prolate spheroidal particle, shear-induced lift force, non-streamwise flow shear, Lagrangian particle tracking.

---

1. Introduction

The derivation of models of shear-induced lift force acting on non-spherical particles in arbitrary non-uniform flow remains a challenging problem through several decades. Saffman (1965, 1968) first derived a model of shear-induced lift force acting on a spherical particle moving through a highly viscous fluid. Harper & Chang (1968) generalised Saffman's calculation to arbitrarily shaped three-dimensional (3D) bodies in linear shear flow by introducing a lift tensor that is calculated via asymptotic methods. Fan & Ahmadi (1995) applied this lift tensor to the calculation of the shear lift force acting on an axisymmetric ellipsoidal particle in linear shear flows. However, the shear lift models listed above are only applicable for linear shear flows. Cui et al. (2018a) proposed a computational method that can extend lift force models that were originally derived for linear shear flow conditions to general flow conditions by performing two coordinate rotations, facilitating the computation of the lift force from the dominant streamwise flow shear. In general, it is unfortunately not possible to transform an arbitrary velocity gradient into a pure (linear) shear flow, since a rotational flow (anti-symmetric tensor), or a pure deformational flow (symmetric tensor, irrotational flow) have intrinsic properties that differ from each other. However, if the particle Reynolds numbers considered are sufficiently small it is reasonable to assume that the flow around a particle is linear and dominated by viscous forces (creeping flow approximation). In this framework, the method proposed by Cui et al. (2018a) can be used for the computation of Saffman-type lift forces on particles through two coordinate transformations. The shear lift force model for prolate spheroidal particles proposed by Cui et al. (2018a) has been verified by means of numerical simulations of a particle moving in Poiseuille flow. However, in general flow conditions, as for example in the well-known benchmark test case of lid-driven cavity flow, the non-streamwise shear also plays an important role and should not be neglected when computing the overall lift force on a particle. The present work aims to extend the shear lift force model (Cui et al., 2018a), developed in Part I, for prolate spheroidal particles taking into account also the non-streamwise flow shear.

The paper is organized as follows. In Sect. 2, by taking into account the non-streamwise flow shear, a novel shear lift force model for prolate spheroidal particles is proposed by employing two coordinate rotations. In Sect. 3, the accuracy and reliability of the proposed novel shear lift force model are verified and validated in Poiseuille and lid-driven cavity flows by comparing it with other Saffman-type lift force models. The paper closes with conclusions.

Notation:. *Tensors* of various order are expressed in bold italic font, i.e. a first-order tensor (vector) and a second-order tensor are denoted by $\boldsymbol{A}$ and $\boldsymbol{B}$, respectively. In a Cartesian coordinate system with base vectors $\boldsymbol{e}_i$ ($i = x, y, z$) they have the coordinate representation $\boldsymbol{A} = A_i \boldsymbol{e}_i$ and $\boldsymbol{B} = B_{ij} \boldsymbol{e}_i \otimes \boldsymbol{e}_j$, respectively, whereby Einstein's summation convention applies for repeated indices. A_i and B_{ij} are the *coefficients* of $\boldsymbol{A}$ and $\boldsymbol{B}$, respectively, in the chosen coordinate system $\boldsymbol{e}_i$. They may be arranged into *coefficient matrices*

$$\mathbf{A} := \begin{bmatrix} A_x \\ A_y \\ A_z \end{bmatrix} \quad \text{and} \quad \mathbf{B} := \begin{bmatrix} B_{xx} & B_{xy} & B_{xz} \\ B_{yx} & B_{yy} & B_{yz} \\ B_{zx} & B_{zy} & B_{zz} \end{bmatrix}$$

whereby bold non-italic font is used for coefficient matrices. Indeed $\mathbf{A}$ is a column matrix, the superscript T denotes transposition so that $\mathbf{A}^T = [A_x, A_y, A_z]$ (a row matrix). In the sequel we restrict ourselves to the use of (local) Cartesian coordinate systems $\boldsymbol{e}_i$ and $\boldsymbol{e}'_i$ that are related via rotation with rotation matrix

$\mathbf{V}$ (or likewise by rotation tensor $\boldsymbol{Q}$), i.e.

$$\boldsymbol{e}'_i = V_{ik}\boldsymbol{e}_k = [V_{lk}\boldsymbol{e}_k \otimes \boldsymbol{e}_l] \cdot \boldsymbol{e}_i =: \boldsymbol{Q} \cdot \boldsymbol{e}_i \quad \text{with} \quad \mathbf{Q} = \mathbf{V}^T.$$

Without loss of generality we will thus only use the corresponding matrix arrangements of tensor coefficients, whereby upon rotation of the coordinate system $\boldsymbol{e}_i$, the corresponding coefficient matrices transform as

$$\mathbf{A}' = \mathbf{V}\,\mathbf{A} \quad \text{and} \quad \mathbf{B}' = \mathbf{V}\,\mathbf{B}\,\mathbf{V}^T.$$

2. The novel shear lift force model for prolate spheroidal particles

Formal studies (Lighthill, 1956a,b; Auton, 1987; Auton et al., 1988; Crowe et al., 2011; Sommerfeld et al., 2008) show that the shear-induced lift force is in the direction of the cross product between the particle slip velocity (i.e. $[\boldsymbol{u}-\boldsymbol{v}]$, where $\boldsymbol{u}$ and $\boldsymbol{v}$ are the fluid velocity at the particle location and the particle velocity, respectively) and the vorticity (i.e. $\boldsymbol{w}$, where $\boldsymbol{w} := \mathrm{curl}\boldsymbol{u}$ is the fluid vorticity (curl of the fluid velocity) at the particle location). The unit direction of the shear-induced lift force is defined in vector notation as

$$\hat{\boldsymbol{u}} = \frac{[\boldsymbol{u}-\boldsymbol{v}] \times \boldsymbol{w}}{|[\boldsymbol{u}-\boldsymbol{v}] \times \boldsymbol{w}|} \equiv \boldsymbol{e}^*_z, \tag{1}$$

and coincides (locally) with the base vector $\boldsymbol{e}^*_z$ of the coordinate system $\boldsymbol{e}^*_i$ $(i = x, y, z)$.

The present shear-induced lift force model is obtained by means of two coordinate rotations. As shown in Fig. 1, the first step is the determination of the rotation matrix $\mathbf{V}^*$, rotating the coefficient (column) matrix $\hat{\mathbf{u}}$ into the coefficient (column) matrix $\mathbf{e}^*_z = [0,\, 0,\, 1]^T$

$$\mathbf{e}^*_z = \mathbf{V}^*\,\hat{\mathbf{u}}. \tag{2}$$

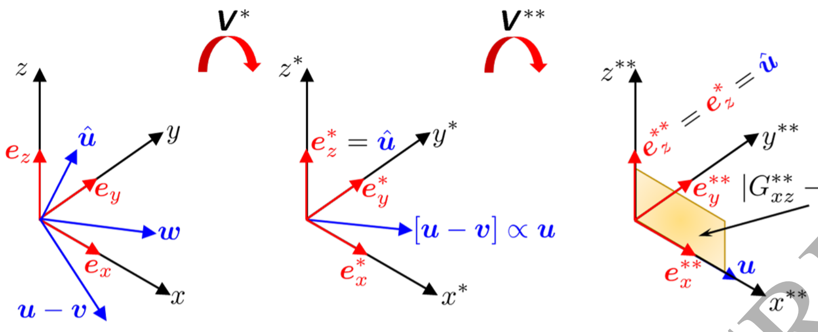

Figure 1: Illustration of the first and second coordinate transformations.

Here $\mathbf{e}_z^*$ and $\hat{\mathbf{u}}$ are the corresponding coefficient (column) matrices of the base vector $\boldsymbol{e}_z^*$ and the unit direction vector $\hat{\boldsymbol{u}}$, respectively. For the efficient construction of the rotation matrix $\mathbf{V}^*$ to rotate one vector into another the method of Möller & Hughes (1999) is used.

Note that $\hat{\boldsymbol{u}}$ is the unit vector of the cross product between the particle slip velocity and the vorticity. In other words, $\hat{\boldsymbol{u}}$ is perpendicular to the plane spanned by vectors $[\boldsymbol{u} - \boldsymbol{v}]$ and $\boldsymbol{w}$. Therefore, in the coordinate system $\boldsymbol{e}_i^*$, $[\boldsymbol{u} - \boldsymbol{v}]$ lies in the x^*-y^* plane and the z^*-component of $[\boldsymbol{u} - \boldsymbol{v}]$ is zero. In the following we make a critical assumption:

Assumption 2. [1]

> The particle slip velocity is parallel to the fluid velocity, i.e. $[\boldsymbol{u} - \boldsymbol{v}] \propto \boldsymbol{u}$ or $\boldsymbol{v} \propto \boldsymbol{u}$ as illustrated in Fig. 2.

In fact, *Assumption 2* is one of the key assumptions of the celebrated Saffman lift (Saffman, 1965, 1968; Stone, 2000). If the particle size is in the micro and submicron range, *Assumption 2* is usually satisfied since gravity plays only a minor role with respect to other forces acting on the particle. Under such a

[1] In the present paper, the numberings of *Assumption* and *Algorithm* start from the second and the third, respectively, in order to distinguish them from the numberings of the companion paper Cui et al. (2018a).

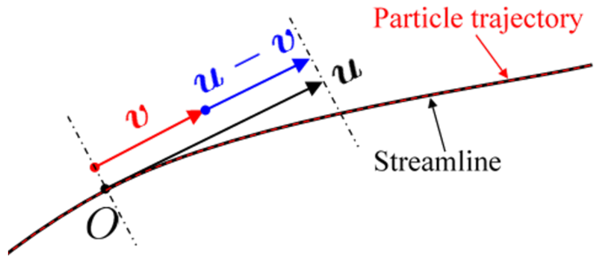

Figure 2: Illustration of *Assumption 2*.

condition, the fluid velocity in the coordinate system $\boldsymbol{e}_i^*$ lies in the x^*-y^* plane with its z^*-component being zero, i.e. $\mathbf{u}^* = \mathbf{V}^*\,\mathbf{u} = [u_x^*,\, u_y^*,\, 0]^T$, where $\mathbf{u}^*$ and $\mathbf{u}$ are the corresponding coefficient (column) matrices of fluid velocities in the coordinate systems $\boldsymbol{e}_i^*$ and $\boldsymbol{e}_i$, respectively.

As shown in Fig. 1, the second coordinate rotation by the rotation matrix $\mathbf{V}^{**}$ rotates the coordinate system $\boldsymbol{e}_i^*$ around the z^*-axis into a new coordinate system $\boldsymbol{e}_i^{**}$, so that the fluid velocity in the new coordinate system $\boldsymbol{e}_i^{**}$ is in the direction of $\boldsymbol{e}_x^{**}$:

$$\mathbf{e}_x^{**} = \mathbf{V}^{**}\,\frac{\mathbf{u}^*}{|\mathbf{u}^*|}, \tag{3}$$

where $\mathbf{e}_x^{**} = [1,\, 0,\, 0]^T$ is the corresponding coefficient (column) matrix of the base vector $\boldsymbol{e}_x^{**}$.

After two coordinate rotations, in the coordinate system $\boldsymbol{e}_i^{**}$, the particle can be considered as moving in a linear shear flow $\mathbf{u}^{**} = \mathbf{V}^{**}\,\mathbf{u}^* = [u_x^{**},\, 0,\, 0]^T$ in the x^{**}-z^{**} plane, with the corresponding shear rate being

$$|G_{xz}^{**} - G_{zx}^{**}|,$$

where G_{xz}^{**} and G_{zx}^{**} are the coefficients of the velocity gradient tensor in the coordinate system $\boldsymbol{e}_i^{**}$, i.e. $\mathbf{G}^{**}$, at the particle location and their indices denote the index of rows and columns of $\mathbf{G}^{**}$, respectively. $\mathbf{G}^{**}$ can be calculated by

$$\mathbf{G}^{**} = \mathbf{V}^{**}\,\mathbf{G}^*\,\mathbf{V}^{**T}, \tag{4}$$

with $\mathbf{G}^* = \mathbf{V}^* \, \mathbf{G} \, \mathbf{V}^{*T}$, where $\mathbf{G}$ and $\mathbf{G}^*$ are the corresponding coefficient matrices of the velocity gradient tensor in the coordinate system $\boldsymbol{e}_i$ and $\boldsymbol{e}_i^*$, respectively.

Therefore, in the coordinate system $\boldsymbol{e}_i^{**}$, the shear lift force can be calculated by using lift models which are devised for linear shear flows. In the case of prolate spheroidal particles, we take as an example the lift force model proposed by Harper & Chang (1968) as a basis.

The novel shear lift force for prolate spheroidal particles is expressed as

$$\mathbf{F}_{SL} = \pi^2 \rho_f a^2 \sqrt{\nu}\, \mathbf{l}, \tag{5}$$

where ρ_f, ν are the fluid density and fluid kinematic viscosity, a is the semi-minor axis of the prolate spheroidal particle, and $\mathbf{l}$ is the coefficient (column) matrix of the lift vector $\boldsymbol{l}$, defined as

$$\mathbf{l} = \sqrt{|G_{xz}^{**} - G_{zx}^{**}|}\, \mathbf{V}^{*T}\, \mathbf{V}^{**T}\, \mathbf{K}^{**}\, \mathbf{L}_{xz}^{**}\, \mathbf{K}^{**}\, \mathbf{V}^{**}\, \mathbf{V}^{*}\, [\mathbf{u} - \mathbf{v}], \tag{6}$$

where $\mathbf{K}^{**} = \mathbf{V}^{**}\, \mathbf{K}^*\, \mathbf{V}^{**T}$ with $\mathbf{K}^* = \mathbf{V}^*\, \mathbf{K}\, \mathbf{V}^{*T}$, and $\mathbf{K}$ and $\mathbf{L}_{xz}^{**}$ are the corresponding coefficient matrices of the (geometric) resistance tensor of the prolate spheroidal particle $\boldsymbol{K}$ in the coordinate system $\boldsymbol{e}_i$ and of the lift tensor $\boldsymbol{L}_{xz}$ in the coordinate system $\boldsymbol{e}_i^{**}$, respectively. $\boldsymbol{K}$ is firstly defined in the particle frame of reference and is then transformed into the inertial frame of reference. In the case of spherical particles, $\mathbf{K} = \mathbf{K}^* = \mathbf{K}^{**} = 6\,\mathbf{I}$. Details on the calculation of $\mathbf{K}$ can be found in Cui et al. (2018a). $\mathbf{L}_{xz}^{**}$ is calculated via asymptotic methods by Harper & Chang (1968) and is expressed as:

$$\mathbf{L}_{xz}^{**} = \begin{bmatrix} A & 0 & B \\ 0 & C & 0 \\ D & 0 & E \end{bmatrix}, \tag{7}$$

where the coefficients of $\mathbf{L}_{xz}^{**}$ are given as

$$A = 0.0501,\ B = 0.0329,\ C = 0.0373,\ D = 0.0182,\ E = 0.0173. \tag{8}$$

The algorithm for calculating the shear lift force acting on a prolate spheroidal particle is summarised as follows:

Algorithm 3.

1. Compute the rotation matrix $\mathbf{V}^*$ by using Eq. 2;
2. Compute the rotation matrix $\mathbf{V}^{**}$ by using Eq. 3;
3. Compute the coefficient matrix $\mathbf{G}^{**}$ of the velocity gradient tensor by using Eq. 4;
4. Compute the shear lift force $\boldsymbol{F}_{SL}$ by using Eqs. 5 - 6.

The accuracy of the present shear lift model depends on how close the flow condition satisfies the conditions in the *Assumption 2*. This can be validated by evaluating the angle between the particle slip velocity and the fluid velocity along the particle trajectory, which is given by (in vector notation)

$$\alpha = \arccos\left(\frac{[\boldsymbol{u}-\boldsymbol{v}]\cdot\boldsymbol{u}}{|[\boldsymbol{u}-\boldsymbol{v}]|\;|\boldsymbol{u}|}\right). \tag{9}$$

This angle is expected to be as small as possible if the conditions in the *Assumption 2* are to be satisfied. Since accuracy requirements among simulation cases are different, the maximum angle for using *Algorithm 3* is not quantitatively defined in the present study.

Remark (Difference between the lift models in Part I and II)**.** *The main difference to the procedure in Part I is the starting point for the two-rotation method. The lift model in Part I first aligns the fluid velocity with the streamwise direction and then two streamwise shear rates are compressed into one shear rate; the present model first aligns* $\boldsymbol{e}_z^*$ *with* $\hat{\boldsymbol{u}}$*, the unit direction of the shear-induced lift force, and then rotates the coordinate system around the* z^**-axis until the fluid velocity is in the direction of* $\boldsymbol{e}_x^{**}$*. Moreover, the lift model in Part I only calculates the streamwise shear* G_{xz}^{**}*, while the present model also takes into account the non-streamwise shear* G_{zx}^{**}*.*

In Sect. 3, the novel shear lift model for prolate spheroidal particles is verified against the established generalised Saffman-type lift force model for spherical particles proposed by Crowe et al. (2011), expressed here in vector notation as

$$\boldsymbol{F}_{SL} = 6.46 \rho_f a^2 \sqrt{\nu} \frac{1}{\sqrt{|\boldsymbol{w}|}} \left[[\boldsymbol{u} - \boldsymbol{v}] \times \boldsymbol{w} \right]. \tag{10}$$

Moreover, previous studies (Miyazaki et al., 1995; Stone, 2000) show that the lift tensor $\boldsymbol{L}_{xz}$ obtained by Harper & Chang (1968) has some (reasonable small) numerical discrepancy with respect to the mobility tensor proposed by Miyazaki et al. (1995), which is obtained in the steady limit of a spherical particle moving in arbitrary linear shear flow. To improve the understanding of the numerical discrepancy between these two tensors, we implement the present method to reconstruct the lift force model of Miyazaki et al. (1995) as follows:

Algorithm 4.

1. Compute the rotation matrix $\mathbf{V}^*$ by using Eq. 2;
2. Compute the rotation matrix $\mathbf{V}^{**}$ by using Eq. 3;
3. Compute the coefficient matrix $\mathbf{G}^{**}$ of the velocity gradient tensor by using Eq. 4;
4. Compute the shear lift force $\boldsymbol{F}_{SL}$ as

$$\mathbf{F}_{SL} = 6\pi \rho_f a^2 \sqrt{\nu} \sqrt{|G^{**}_{xz} - G^{**}_{zx}|}\, \mathbf{V}^{*T}\, \mathbf{V}^{**T}\, \mathbf{L}^{**}_m\, \mathbf{V}^{**}\, \mathbf{V}^* \left[\mathbf{u} - \mathbf{v}\right], \tag{11}$$

where the corresponding coefficient matrix of the mobility tensor given by Miyazaki et al. (1995) is

$$\mathbf{L}^{**}_m = \begin{bmatrix} 0.327 & 0 & 0.944 \\ 0 & 0.577 & 0 \\ 0.343 & 0 & 0.0735 \end{bmatrix}. \tag{12}$$

In the case of spherical particles, the z^{**}-components of the lift force induced by the velocity difference in the x^{**}-direction calculated by the lift tensor and the mobility tensor agree with the result of Saffman (Saffman, 1965, 1968), i.e. $36\,\pi^2\,D = 6\,\pi \times 0.343 = 6.46$, which corresponds to the finding of Harper & Chang (1968), Fan & Ahmadi (1995) and Miyazaki et al. (1995).

The above lift force models, as well as particle tracking algorithms presented in Cui et al. (2018a), have been implemented into MATLAB® and OpenFOAM®. The implicit Euler backward scheme was applied in both codes, which were used in the computational studies for numerical verification and validation of the novel shear lift force model.

3. Numerical verification and validation of the novel shear lift force model for prolate spheroidal particles in Poiseuille and lid-driven cavity flows

3.1. Numerical verification of the transport of a prolate spheroidal particle in Poiseuille flow

Under *Assumption 2*, in the coordinate system $\boldsymbol{e}_i^{**}$, only the x^{**}-component of the particle slip velocity is non-zero, i.e. $[\mathbf{u}^{**} - \mathbf{v}^{**}] = [u_x^{**} - v_x^{**},\, 0,\, 0]^T$. In the case of spherical particles, the coefficients B, C and E have no influence on the lift force, and only the coefficients A and D make contributions to the lift. It is important to understand the accuracy and the reliability of the present shear lift model. In this section, the present shear lift model is compared with the shear lift model proposed in Part I (Cui et al., 2018a) in a Poiseuille flow. The complete simulation setup of the Poiseuille flow has already been described in Sect. 3.1 of Cui et al. (2018a), and thus will not be repeated here.

In the simulation of Poiseuille flow, the particles are placed at different circumferential positions in the pipe, whereby their radial distances to the pipe centreline are kept constant. In the present study, we use the most representative initial particle positions, e.g. P_1 and P_4 (with the detailed information listed in Table 1 & 2 of the companion paper), as these two initial positions can well capture the sequential transformations $\mathbf{V}^*$ and $\mathbf{V}^{**}$ for calculating the shear lift force (Cui et al., 2018a). Fig. 3 plots trajectories of a single spherical particle computed using different shear lift force models. Among these shear-induced lift force models, the lift force model proposed by Cui et al. (2018a) is considered as the benchmark model. This is because the generalised Saffman lift only accounts for the lift induced by the relative motion between the fluid and the particle in the streamwise direction (captured by the coefficient D), but neglects the inertia effect of the Stokes drag (captured by the coefficients A, C and E, see Cui et al. (2018a) for more details) as well as the particle motion in non-streamwise directions (captured by the coefficient B). As depicted in Fig. 3, the difference between the present model and the benchmark model is very small and is much less than the difference between the generalised Saffman-type lift force model proposed by Crowe et al. (2011) and the benchmark model. This implies that the influence of the coefficients B, C and E on the particle motion is small. However, the influence of the coefficient A on the particle motion is relatively large compared to the influence of other coefficients. In the case of prolate spheroidal particles with the aspect ratio $\lambda = 10$ (where $\lambda = b/a$ with b the semi-major axis of the prolate spheroidal particle), the discrepancy in the computed radial position between the present shear lift model and the benchmark model, as highlighted in Fig. 4, steadily increases along the particle trajectory, which is to be expected due to the time marching integration scheme, and can, therefore, be considered as acceptable. By changing the initial particle position from P_1 to P_4, the computational results between two initial particle positions are identical (see Fig. 3 and 4), proving the validity of the sequential transformations $\mathbf{V}^*$ and $\mathbf{V}^{**}$ for calculating the shear lift force.

3.2. Comparing the present model with direct numerical simulation results

To the best of our knowledge, there is no available data from the literature to validate the present model directly. The difficulty lies in the fact that, from both the experimental measurement and direct numerical simulation (DNS) point of view, the simulated or measured fluid dynamic forces are only one single fluid force. Unfortunately, one cannot divide the fluid force into different contribu-

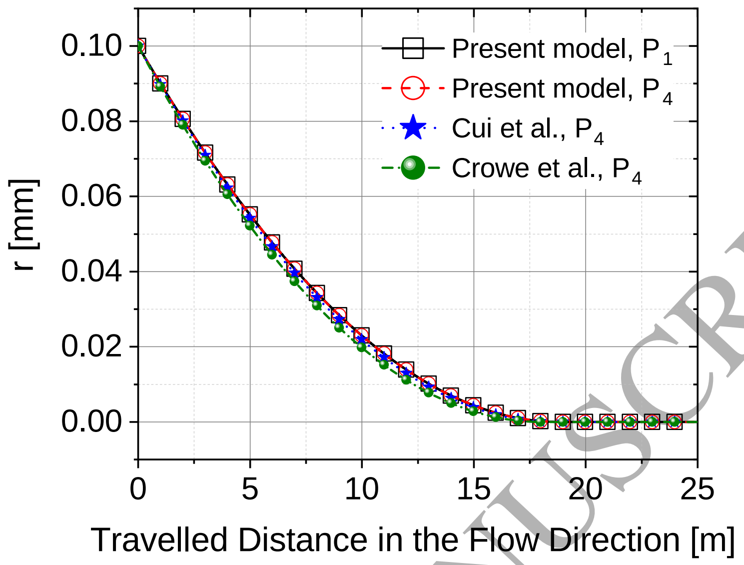

Figure 3: Translational motion of a spherical particle in Poiseuille flow for different shear lift force models and initial positions (tracking time: $50\,s$, time step: $10\,\mu s$, $D_p = 20\,\mu m$).

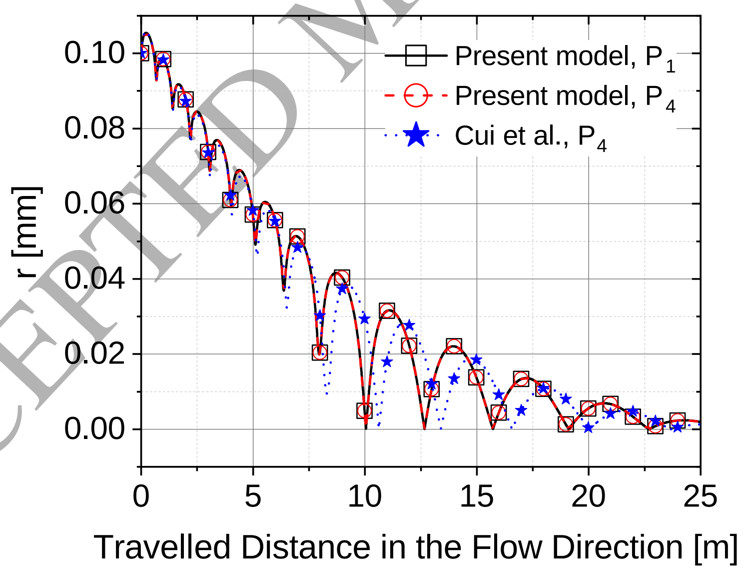

Figure 4: Translational motion of a prolate spheroidal particle in Poiseuille flow for different initial positions and aspect ratios (tracking time: $50\,s$, time step: $10\,\mu s$, $\lambda = 10$, $D_p = 20\,\mu m$).

tion, such as the drag, the Magnus lift, the profile lift, the lift due to viscous force (i.e. Saffman-type lift) and the lift due to non-uniform pressure distribution around the particle. In most studies (Zastawny et al., 2012; Ouchene et al., 2016; Sanjeevi et al., 2018), where the particle is fully-resolved, only the profile lift of a stationary non-spherical particle in an uniform flow was calculated by varying the angle of incidence and the Reynolds number.

In order to obtain the shear-induced lift force one can calculate the difference in lift between a uniform flow case and a linear shear flow case. Although the lift due to the non-uniform pressure distribution is also added up to the final results, the lift will be dominated by the viscous force if the particle is "small enough". Hölzer & Sommerfeld (2009) calculated the lift force acting on a stationary sphere and spheroid in a linear shear Couette flow, and they found that the lift acting on the particle is very sensitive to the distance between the top and bottom walls, and in this case a good agreement with Saffman's solution cannot be obtained. Moreover, Saffman assumes that the particle is free-rotating. Bagchi & Balachandar (2002) reported that the lift force for a free-rotating sphere in linear shear flow is larger than in the case of a stationary particle, since the streamline patterns for these two cases are different. Meanwhile, when a particle is in a torque-free condition, the Magnus lift takes effect. However, the Magnus lift can be neglected if Saffman's assumptions are satisfied (Saffman, 1965), i.e. $Re_p = D_p\,|\mathbf{u}-\mathbf{v}|/\nu \ll 1$, $Re_G = D_p^2\,|\mathbf{G}|/\nu \ll 1$ and $Re_p \ll Re_G^{1/2}$. As a consequence, it is computationally very expensive to validate the present model by using DNS.

In this section, we first calculate the lift force of a free-rotating (without translation) sphere in Poiseuille flow. The geometry and boundary conditions as well as particle properties of the simulation are the same as used in Sect. 3.1. The intial particle location of P_1 is considered. The DNS is performed by using finite volume method based open source code OpenFOAM®. Fig. 5 plots the mesh around the particle. In total 4.8 million cells are generated. The dimensionless parameters used in this section are the drag and lift coefficients,

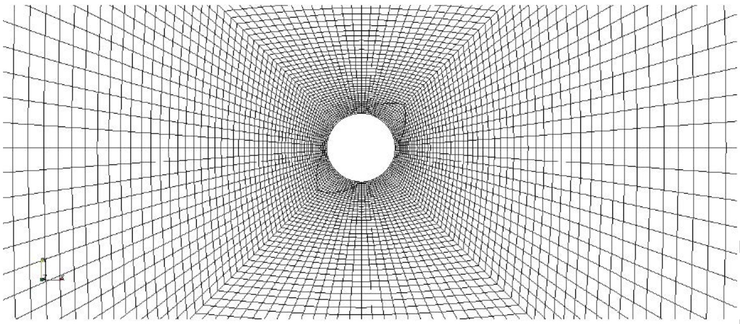

Figure 5: The mesh around a fully-resolved free-rotating spherical particle.

being defined by

$$c_D = \frac{F_{D,s} + F_{SL,s}}{\frac{1}{2}\rho_f |\boldsymbol{u} - \boldsymbol{v}|^2 \frac{\pi}{4} D_p^2} \tag{13}$$

$$c_L = \frac{F_{D,p} + F_{SL,p}}{\frac{1}{2}\rho_f |\boldsymbol{u} - \boldsymbol{v}|^2 \frac{\pi}{4} D_p^2} \tag{14}$$

where $F_{D,s}$ and $F_{SL,s}$ are the components of Brenner's drag and the present model, respectively, in the direction of the slip velocity, and $F_{D,p}$ and $F_{SL,p}$ are the components of Brenner's drag and the present model, respectively, in the direction perpendicualr to the slip velocity.

As shown in Fig. 6a, the drag coefficients calculated by the DNS and the present model (i.e. $F_{D,s} + F_{SL,s}$) show excellent agreement. We observe a small numerical discrepancy in lift coefficents calculated by the present model (i.e. $F_{D,p} + F_{SL,p}$) and the DNS (see Fig. 6b). In addition, this numerical discrepancy decreases with decreasing particle shear Reynolds numbers, which confirms the correctness of Saffman's assumption.

As aforementioned, Hölzer & Sommerfeld (2009) calcualte the drag and lift coefficients acting on a stationary spheroid in a linear shear flow. However, most of their simulations do not satisfy Saffman's assmuptions, only one simulation case with $Re_p = 0.3$, $Re_G = 0.096$ and $Re_G^{1/2} = 0.3098$ is marginally acceptable. In this case, the aspect ratio of the prolate spheroid is 1.5. Fig. 7 compares the lift and drag coefficients calculated by the present model and the Lattice Boltzmann simulation results of Hölzer & Sommerfeld (2009). The shapes of

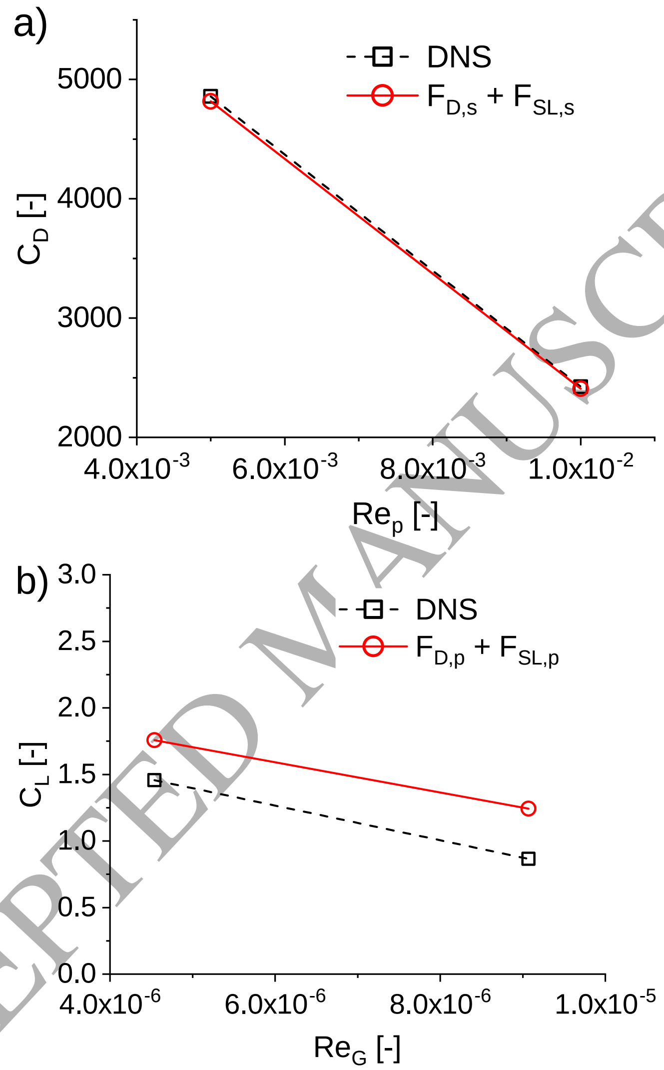

Figure 6: Drag and lift coefficients of a free-rotating sphere moving in Poiseuille flow calculated by DNS and the present model; *a*) Drag coefficient as a function of particle Reynolds number; *b*) Lift coefficient as a function of particle shear Reynolds nubmer.

curves of the drag and lift coefficients as a function of incidence angle for the two results show a good agreement. The difference in drag between the two results is small and acceptable, whereas the lift coefficient calculated by the present model is higher than the results of Hölzer & Sommerfeld (2009). This is mainly because the assumption of $Re_p \ll Re_G^{1/2}$ is not satisfied. In addition, Hölzer & Sommerfeld (2009) under predicted the Saffman lift since the size of fluid domain has a large influence on the shear-induced lift.

3.3. Numerical verification of the transport of a prolate spheroidal particle in lid-driven cavity flow

The lid-driven cavity flow is a well-known benchmark problem for viscous incompressible fluid flows. Tsorng et al. (2008) investigated the behaviour of macroscopic rigid particles suspended in a fully three-dimensional viscous flow in a closed cubic cavity. Cui et al. (2018b) numerically calculated the flow field by applying the same setup as used in Tsorng et al. (2008). The cavity is a cubic domain with the edge length $L = 0.1\,m$. The fluid density is $1210\,kg/m^3$, the kinematic fluid viscosity is $17.3\,mm^2/s$, and with the upper wall velocity $U_0 = 0.0813\,m/s$ the flow Reynolds number is 470. The flow streamlines have been computed in Cui et al. (2018b). For convenience Fig. 8 reviews the computed flow patterns.

The longitudinal plane $y/L \approx 0.4$ (red line in Fig. 8b) was chosen for the particle tracking because it features at its upper downstream corner an open pathway linking the primary eddy to the downstream secondary eddy (Tsorng et al., 2008). The initial position of the particle is $[0.5L,\, 0.4L,\, 0.95L]^T$ with its primary axis b pointing in the z-direction. The initial particle velocity is equal to the fluid velocity. The selected volume equivalent particle diameter is $D_p = 100\,\mu m$, and the particle density is $2560\,kg/m^3$. The fluid forces acting on the particle are Brenner's drag (Brenner, 1963) and the lift force due to various shear-induced lift force models (Miyazaki et al., 1995; Crowe et al., 2011; Cui et al., 2018a). The hydrodynamic drag force proposed by Brenner is applicable to the creeping flow regime (Stokes regime) with small Reynolds

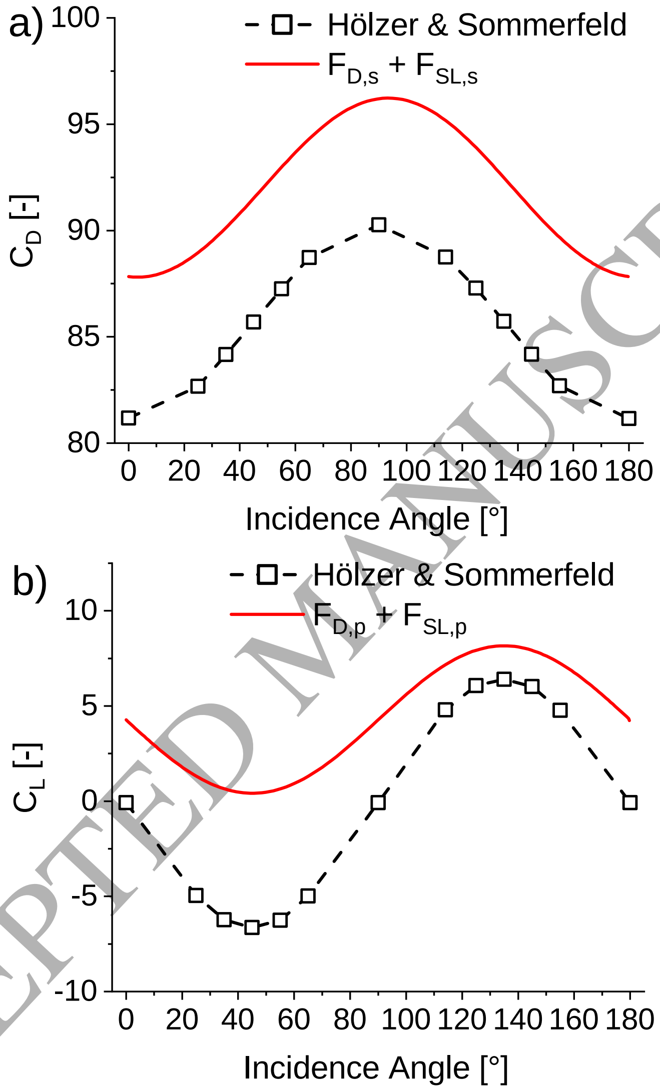

Figure 7: Drag and lift coefficients of a stationary prolate spheroid in a linear shear flow calculated by DNS and the present model; *a*) Drag coefficient as a function of incidence angle; *b*) Lift coefficient as a function of incidence angle.

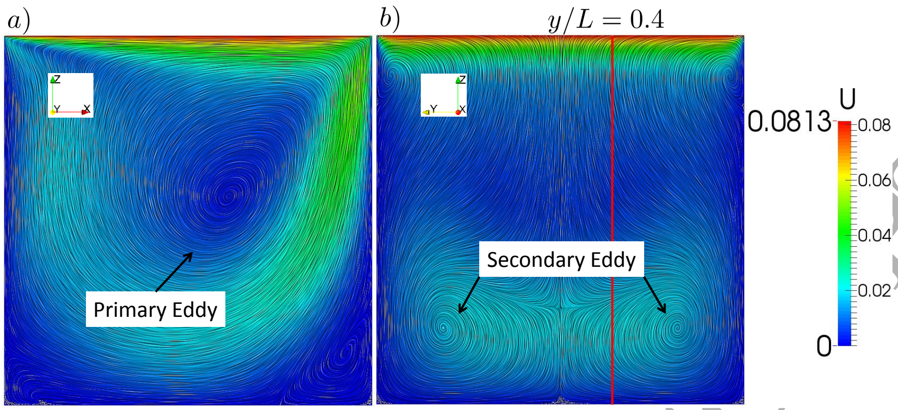

Figure 8: Numerically computed flow streamlines of a 3D lid-driven cavity flow in a cube; a) the longitudinal plane $y/L = 0.4$; b) the central transverse plane $x/L = 0.5$; the red line indicates the plane of particle tracking $y/L = 0.4$; U is the magnitude of the fluid velocity ($Re = 470$, the dimension of the domain: $L = 0.1\,m$) (Cui et al., 2018b).

numbers (Fan & Ahmadi, 1995). The solution of Brenner is derived for a particle approaching an infinitely extended solid boundary. However, in the lid-driven cavity, Brenner's drag becomes incorrect when the particle moves close to the corner. The major repulsive force acting on the particle may be due to the corner singularity which was not taken into account by the solution of Brenner. At the beginning of this section, the lift force acting on the particle along the particle trajectory is only calculated but not taken into account when computing the trajectory of a particle. In this way, the particle trajectories are identical for all computed cases which allowed us to evaluate and better understand the differences between various shear-induced lift models. In addition, when the particle approaches to the vicinity of the wall, the influence of the presence of the wall on the shear-induced lift force is considered to be important. In the case of spherical particles, McLaughlin (1993) extended Saffman's work to account for presence of the walls. However, in the case of prolate spheroidal particles, there are no available models so far. Therefore, we have not taken the wall effect into account in this section.

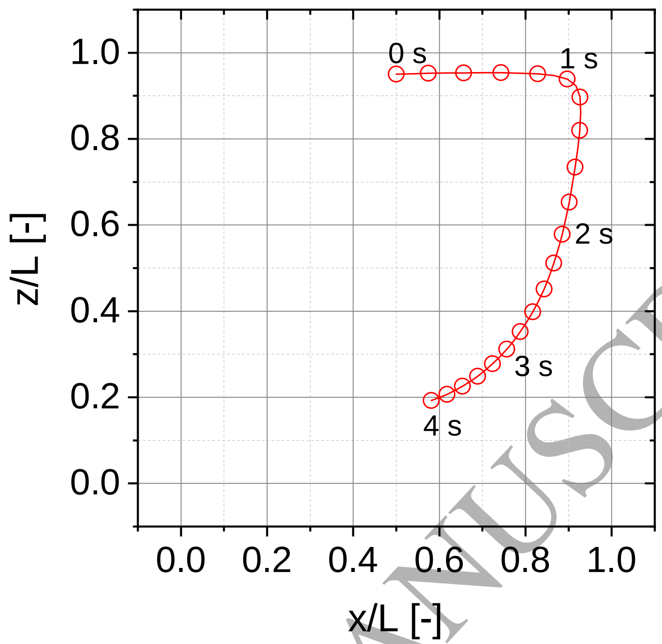

Figure 9: The translational motion of a spherical particle in lid-driven cavity flow (tracking time: $4\,s$, time step: $10\,\mu s$, $D_p = 100\,\mu m$).

The trajectory of a spherical particle moving in a lid-driven cavity flow, under the action of the Brenner's drag and the gravity reduced by buoyancy, is presented in Fig. 9. The total simulation time is $4\,s$. The numbers along the trajectory in Fig. 9 indicate the particle locations at corresponding times and the time intervals between two neighbouring points are identical (i.e. $0.2\,s$). As the considered lift force models are all of the Saffman-type, in addition to *Assumption 2*, the Saffman's assumptions of $Re_p \ll 1$ and $Re_G \ll 1$ as well as $Re_p \ll Re_G^{1/2}$ are required. The computational results of these dimensionless parameters along the particle trajectory of Fig. 9 are plotted in Fig. 10, from which the conclusion can be made that the above three requirements are reasonably satisfied.

As aforementioned, the lift tensor (Harper & Chang, 1968) and the mobility tensor (Miyazaki et al., 1995) not only produce the lift component in the

ACCEPTED MANUSCRIPT

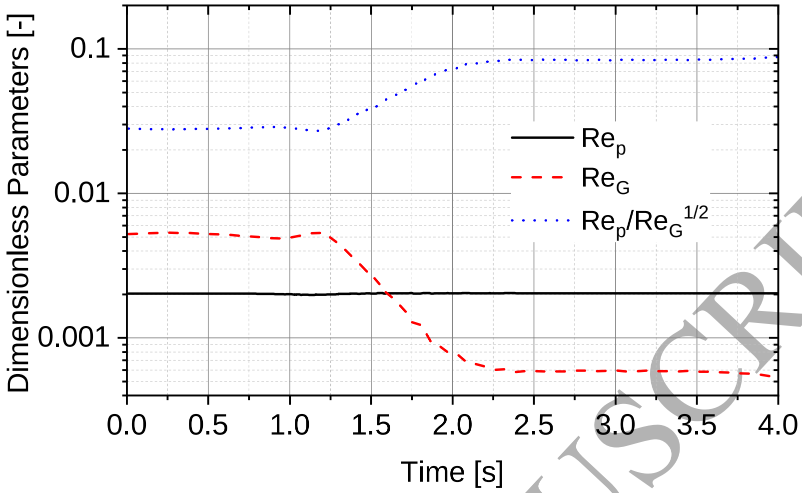

Figure 10: Time evolution of dimensionless parameters of a spherical particle moving in the lid-driven cavity flow (tracking time: $4\,s$, time step: $10\,\mu s$, $D_p = 100\,\mu m$).

non-streamwise direction but also yield the lift component in the streamwise direction. On the contrary, the generalised Saffman lift by Crowe et al. (2011) only calculates the lift in the non-streamwise direction. Therefore, the comparison of different lift models requires separating the lift force (i.e. $\boldsymbol{F}_{SL}$) into a streamwise component (i.e. $\boldsymbol{F}_{SL,s}$) and a component that is perpendicular to the streamwise direction (i.e. $\boldsymbol{F}_{SL,p}$). The magnitudes of $\boldsymbol{F}_{SL,s}$ and $\boldsymbol{F}_{SL,p}$ can be calculated by

$$F_{SL,s} = \frac{\boldsymbol{F}_{SL} \cdot [\boldsymbol{u} - \boldsymbol{v}]}{|\boldsymbol{u} - \boldsymbol{v}|} \quad \text{and} \quad F_{SL,p} = \sqrt{|\boldsymbol{F}_{SL}|^2 - F_{SL,s}^2} \tag{15}$$

The computational results of lift components $F_{SL,p}$ and $F_{SL,s}$ by using different shear-induced lift force models are plotted in Fig. 11 and 12, respectively. A detailed comparison of different lift models leads to the following conclusions:

(i) Difference between the *present model* and the lift model of *Miyazaki et al.*:

The present lift model takes the lift tensor proposed by Harper & Chang (1968) as a basis, whereas the generalised lift model of Miyazaki et al.

(1995) uses the mobility tensor. Therefore, in the case of spherical particles, the difference between the two models lies in the difference between the values of the coefficients of the two tensors. The computational results of $F_{SL,p}$ between the two lift models shows an excellent agreement (see Fig. 11), since $6\pi D = 0.343$, which is exactly the z, x-component of $\mathbf{L}_m$. In the streamwise direction, $6\pi A = 0.944$ which is higher than the x, x-component of $\mathbf{L}_m$, leading to a numerical discrepancy in $F_{SL,s}$ as shown in Fig. 12. However, the ratio between $F_{SL,s}$ and the Stokes drag is proportional to Re_G and is rather small (see Fig. 10). Therefore, this numerical discrepancy in $F_{SL,s}$ between the two models is reasonable small and does not affect the particle motion.

(ii) Difference between the *present model* and the lift model of *Crowe et al.*:

The main difference between these two lift models lies in the calculation of $F_{SL,s}$. The lift model proposed by Crowe et al. (2011) does not take into account the $F_{SL,s}$, whereas the present model calculates $F_{SL,s}$ by the coefficient A in the lift tensor. As shown in Fig. 12, the computational results of $F_{SL,p}$ of the two lift models show a good agreement. In fact, if we replace $|G^{**}_{xz} - G^{**}_{zx}|$ in Eq. 6 with the magnitude of vorticity (i.e. $|\boldsymbol{w}|$), the present model becomes identical to the lift model of *Crowe et al.* for calculating the $F_{SL,p}$. Fig. 13 compares values of $|G^{**}_{xz} - G^{**}_{zx}|$ and $|\boldsymbol{w}|$ along the particle trajectory. The numerical discrepancy, originating mainly in not satisfying the condition of *Assumption 2*, exists but is very small, as can be depicted from Fig. 14, where a plot of the angle between the slip velocity vector and the fluid velocity vector along the particle trajectory is presented. The maximum value reaches up to three degrees, however, since the computational results by the present model agree well with the results of *Crowe et al.*, the magnitude of three degrees is acceptable. In addition, Fig. 14 proves that the particle aspect ratio has insignificant influence on the magnitude of this angle. Although the numerical discrepancy between $|G^{**}_{xz} - G^{**}_{zx}|$ and $|\boldsymbol{w}|$ is very small (see Fig. 13), it is still an open question

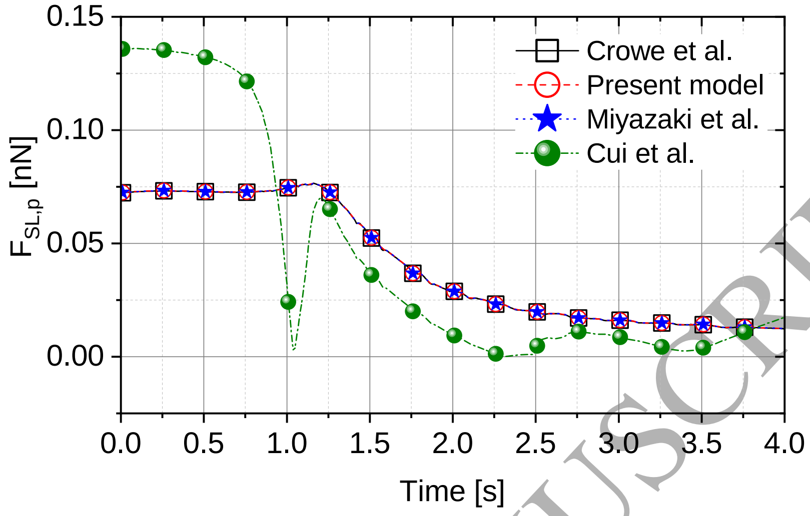

Figure 11: Time evolution of the lift component perpendicular to the flow direction of a spherical particle moving in the lid-driven cavity flow for different shear lift models (tracking time: $4\,s$, time step: $10\,\mu s$, $D_p = 100\,\mu m$).

whether $|G^{**}_{xz} - G^{**}_{zx}|$ can be replaced by $|\boldsymbol{w}|$ or not.

(iii) Difference between the *present model* and the lift model of *Cui et al.*:

In lid-driven cavity flows, the non-streamwise flow shear also plays an important role. The differences in results between the present model and the lift model proposed by *Cui et al.* are obvious, meaning that the lift model proposed by Cui et al. (2018a) is not suited for this situation.

In the case of prolate spheroidal particles, the particle rotates due to the flow resistance and its primary axis b tends to align with the flow direction, where the particle with this orientation angle experiences a minimum drag (Cui et al., 2018a). Under such a condition, as shown in Fig. 15, the magnitude of the shear-induced lift force is actually increased since at this orientation angle the cross-section area of the prolate spheroidal particle is the largest in the direction perpendicular to the streamwise direction.

Finally, the influence of the shear-induced lift force on the particle trajectory

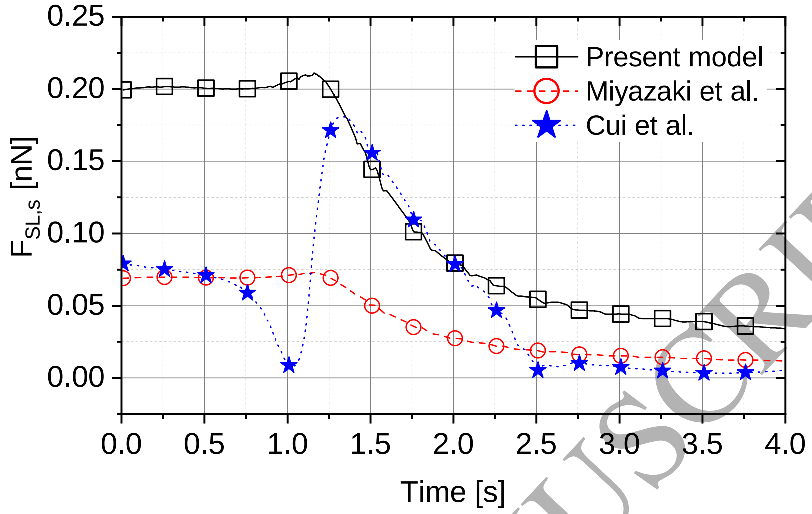

Figure 12: Time evolution of the lift component in the streamwise direction of a spherical particle moving in the lid-driven cavity flow for different shear lift models (tracking time: $4\,s$, time step: $10\,\mu s$, $D_p = 100\,\mu m$).

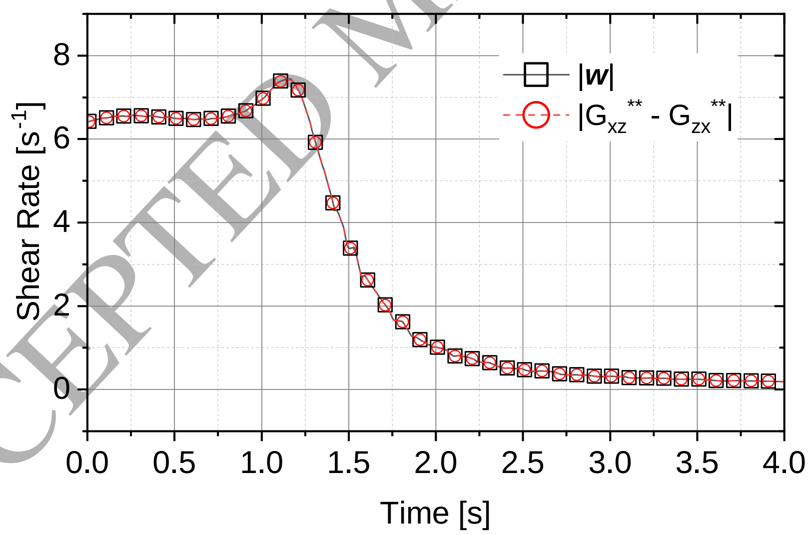

Figure 13: Time evolution of the shear rates at the coordinate system $\boldsymbol{e}_i^{**}$ and the magnitude of vorticity along the particle trajectory in the lid-driven cavity flow (tracking time: $4\,s$, time step: $10\,\mu s$, $D_p = 100\,\mu m$).

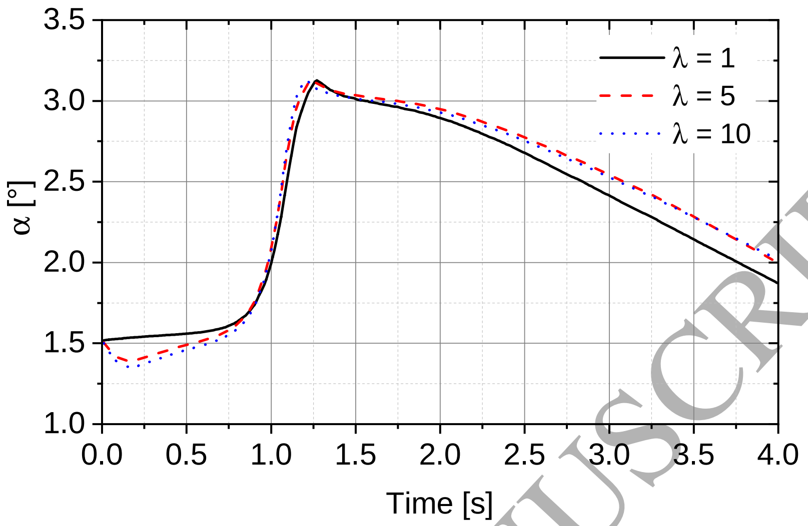

Figure 14: Time evolution of the angle between the particle slip velocity and the fluid velocity of a spherical particle in the lid-driven cavity flow (tracking time: $4\,s$, time step: $10\,\mu s$, $D_p = 100\,\mu m$).

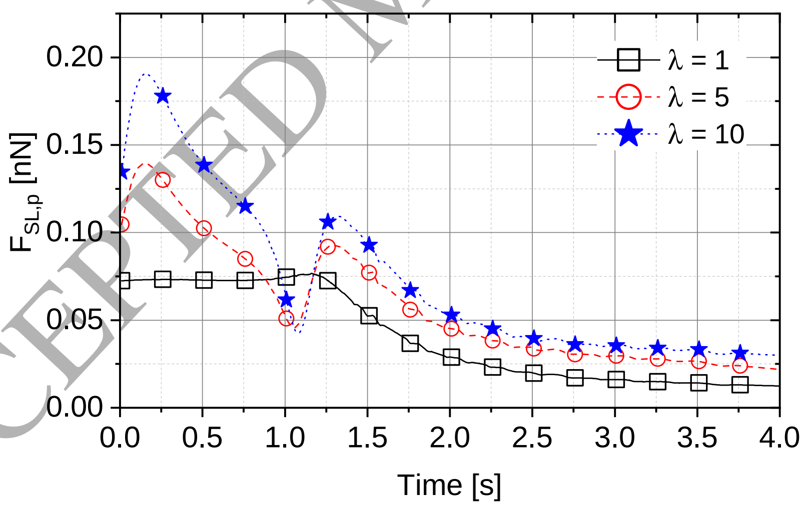

Figure 15: Time evolution of the lift component perpendicular to the flow direction of a prolate spheroidal particle moving in lid-driven cavity flow for different aspect ratios (tracking time: $4\,s$, time step: $10\,\mu s$, $D_p = 100\,\mu m$).

is studied in Fig. 16. The entire simulation time is $100\,s$, and the time intervals between two neighbouring points are $2\,s$. Fig. 16a plots the entire time range, and Fig. 16b shows the time period between $80\,s$ and $100\,s$ in order to emphasise the difference between the curves. Computation of the particle trajectory in this case includes the action of the lift force on the particle. In the case of spherical particles, the influence of the shear-induced lift force on the particle motion is weak but evident as shown in Fig. 16b. The difference in results between the case without lift (black square) and the case using the lift of Crowe et al. (purple sphere) is very small, meaning that the lift force caused by the coefficient D plays minor role on particle trajectory. The influence of shear-induced lift force on the particle trajectory is mainly caused by the inertia effect of the Stokes drag (i.e. diagonal components of the lift tensors) as illustrated by the cases using the lift of Miyazaki et al. (olive triangle) and the present model (red circle). Fig. 17 and Fig. 18 plot the magnitude of the shear rate and the lift components (i.e. $F_{SL,s}$ and $F_{SL,p}$) calculated by the present model, respectively, along the particle trajectory. $F_{SL,s}$ is proportional to the $F_{SL,p}$ since in the case of spherical particles only the coefficients A and D of the lift tensor are taken into account. By comparing Fig. 17 with Fig. 18, as expected, the magnitude of lift components is largely influenced by the shear rate. In the case of prolate spheroidal particles, the particle trajectory changes significantly when increasing the aspect ratio from 1 to 10. The particle tends to align its major axis b with the flow direction. Under such a condition, the drag decreases and the lift increases (see Fig. 15) due to the change of the cross-section area with respect to the flow direction.

4. Conclusions

The present paper proposes a novel shear-induced lift force model for prolate spheroidal particles in arbitrary non-uniform flow, which takes into account the non-streamwise flow shear and can be used for Lagrangian particle tracking. The particle Reynolds number considered in the present study is very small

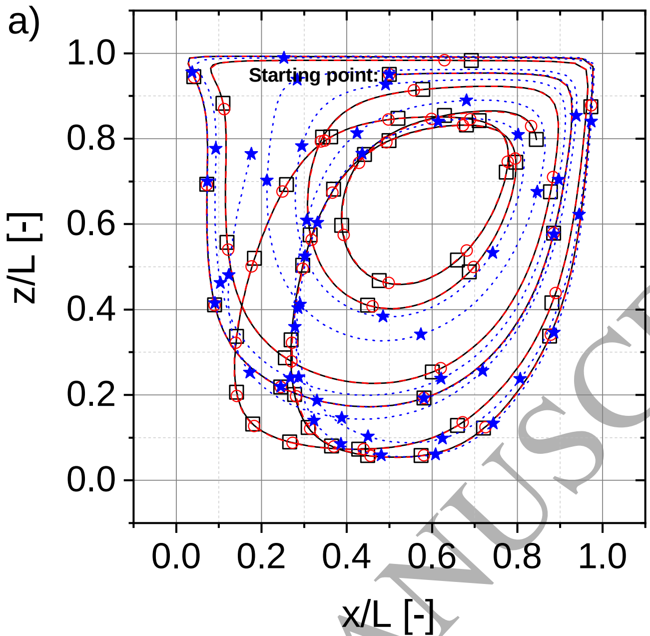

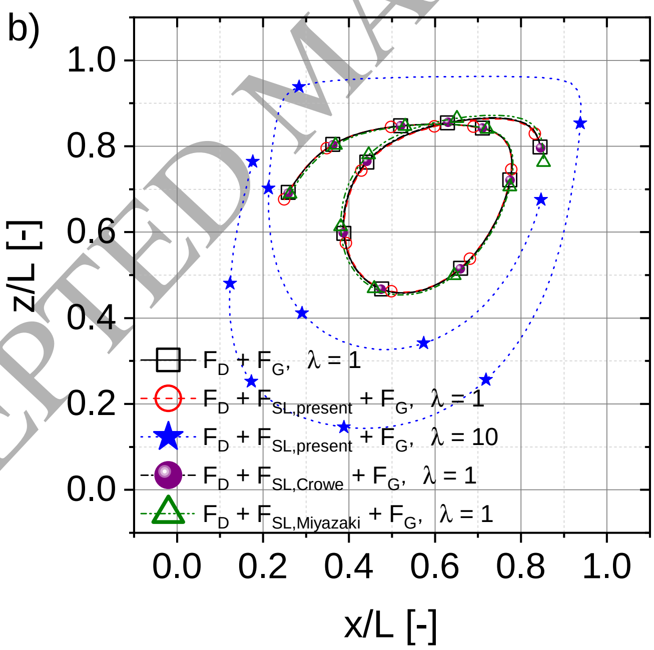

Figure 16: The translational motion of a particle in the lid-driven cavity flow taking into account the shear-induced lift force; a): time period $0\,s - 100\,s$; b): time period $80\,s - 100\,s$ (tracking time: $100\,s$, time step: $10\,\mu s$, $D_p = 100\,\mu m$).

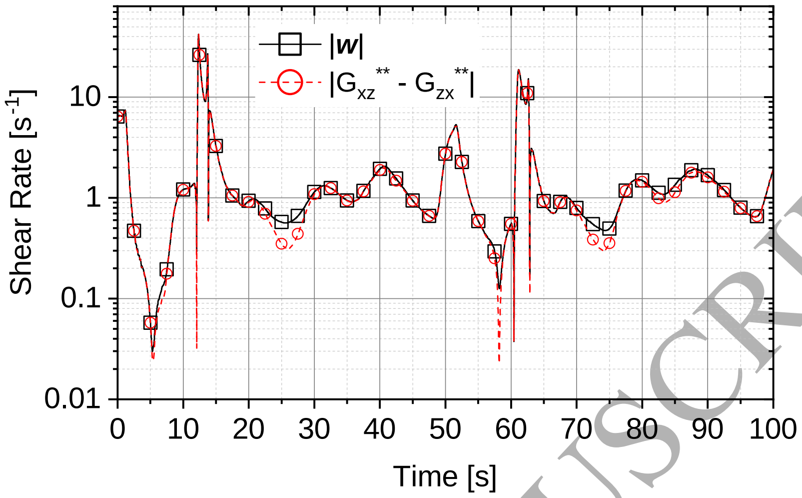

Figure 17: Time evolution of the shear rates at the coordinate system $\boldsymbol{e}_i^{**}$ and the magnitude of vorticity along the particle trajectory; the spherical particle is tracked by including the action of the lift force on the particle calculated by the present model (tracking time: $100\,s$, time step: $10\,\mu s$, $D_p = 100\,\mu m$).

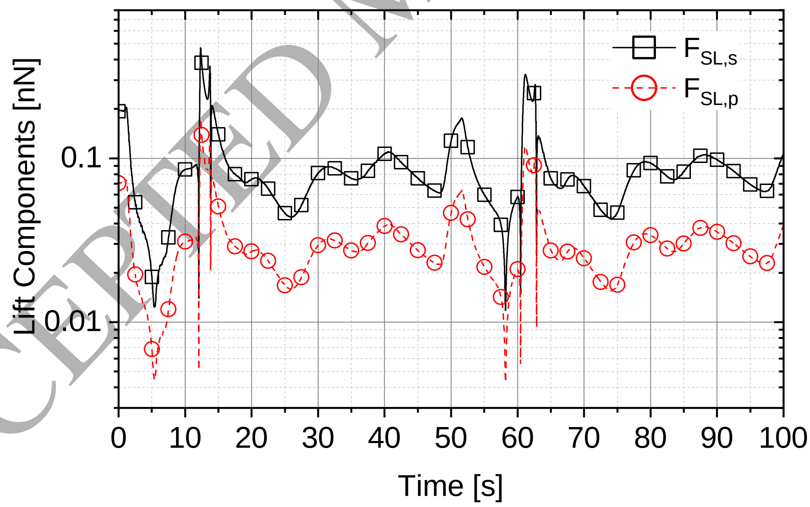

Figure 18: Time evolution of lift components of a spherical particle moving in lid-driven cavity flow including the action of the lift force on the particle calculated by the present model (tracking time: $100\,s$, time step: $10\,\mu s$, $D_p = 100\,\mu m$).

(creeping flow approximation), so that the flow around the particle is assumed to be linear and dominated by viscous forces. By employing two coordinate rotations, the lift force in the coordinate system $\boldsymbol{e}_i^{**}$ can be computed by using any lift force model that is devised for linear shear flows. The first rotation aligns the base vector $\boldsymbol{e}_z^*$ with the lift direction $[\boldsymbol{u} - \boldsymbol{v}] \times \boldsymbol{w}$. By assuming the particle slip velocity is parallel to the fluid velocity (i.e. one of the Saffman's crucial assumptions), the fluid velocity is perpendicular to the lift direction and lies in the x^*-y^* plane. Therefore, the second rotation around the z^*-axis is adopted to align the fluid velocity (or the streamwise direction) with the base vector $\boldsymbol{e}_x^{**}$, for which the lift model of Harper & Chang (1968) can directly be applied.

The accuracy of the present shear lift force model is verified by comparison with the lift model proposed in Part I (Cui et al., 2018a), which is devised for fluid flows dominated by streamwise flow shear, in the case of a Poiseuille flow. In the case of spherical particles, the difference between the two lift models are very small, implying that the coefficients B, C and E have much less influence on the lift than the coefficients A and D of the lift tensor (Harper & Chang, 1968). In the case of prolate spheroidal particles with $\lambda = 10$, the numerical discrepancy between the two lift models increases but is still reasonably small. The ability of the present lift force model for taking into account the non-streamwise flow shear is validated by comparing it with an established generalised Saffman-type lift force model proposed by Crowe et al. (2011) in the 3D lid-driven cavity flow. The lift components perpendicular to the streamwise direction produced by the two lift models show a good agreement. In addition, we found that the computational results for $|G_{xz}^{**} - G_{zx}^{**}|$ along the particle trajectory are very close to the results of $|\boldsymbol{w}|$. However, it is still an open question whether it's physically justified to replace $|G_{xz}^{**} - G_{zx}^{**}|$ with $|\boldsymbol{w}|$ or not. Moreover, we found that the lift model in the companion paper (Cui et al., 2018a) has a limited applicability for the case of the lid-driven cavity flow. Only in fluid flows which are dominated by the streamwise shear, the lift model in Cui et al. (2018a) is more accurate; in other cases, it is advised to use the present shear-induced lift force model.

Acknowledgement: the authors thank the Deutsche Forschungsgemeinschaft for the financial support in the framework of the project STE 544/58.

Declarations of interest: none.

References

References

Auton, T. R. (1987). The lift force on a spherical body in a rotational flow. *Journal of Fluid Mechanics*, *183*, 199. doi:10.1017/s002211208700260x.

Auton, T. R., Hunt, J. C. R., & PrudHomme, M. (1988). The force exerted on a body in inviscid unsteady non-uniform rotational flow. *Journal of Fluid Mechanics*, *197*, 241. doi:10.1017/s0022112088003246.

Bagchi, P., & Balachandar, S. (2002). Effect of free rotation on the motion of a solid sphere in linear shear flow at moderate re. *Physics of Fluids*, *14*, 2719–2737. doi:10.1063/1.1487378.

Brenner, H. (1963). The stokes resistance of an arbitrary particle. *Chemical Engineering Science*, *18*, 1–25. doi:10.1016/0009-2509(63)80001-9.

Crowe, C. T., Schwarzkopf, J. D., Sommerfeld, M., & Tsuji, Y. (2011). *Multiphase Flows with Droplets and Particles*. CRC Press.

Cui, Y., Ravnik, J., Hriberšek, M., & Steinmann, P. (2018a). A novel model for the lift force acting on a prolate spheroidal particle in an arbitrary non-uniform flow. part i. lift force due to the streamwise flow shear. *International Journal of Multiphase Flow*, *104*, 103–112. doi:10.1016/j.ijmultiphaseflow.2018.03.007.

Cui, Y., Ravnik, J., Hriberšek, M., & Steinmann, P. (2018b). On constitutive models for the momentum transfer to particles in fluid-dominated two-phase flows. In *Advanced Structured Materials* (pp. 1–25). Springer International Publishing. doi:10.1007/978-3-319-70563-7_1.

Fan, F.-G., & Ahmadi, G. (1995). A sublayer model for wall deposition of ellipsoidal particles in turbulent streams. *Journal of Aerosol Science*, *26*, 813–840. doi:10.1016/0021-8502(95)00021-4.

Harper, E. Y., & Chang, I.-D. (1968). Maximum dissipation resulting from lift in a slow viscous shear flow. *Journal of Fluid Mechanics*, *33*, 209. doi:10.1017/s0022112068001254.

Hölzer, A., & Sommerfeld, M. (2009). Lattice boltzmann simulations to determine drag, lift and torque acting on non-spherical particles. *Computers & Fluids*, *38*, 572–589. doi:10.1016/j.compfluid.2008.06.001.

Lighthill, M. J. (1956a). Drift. *Journal of Fluid Mechanics*, *1*, 31. doi:10.1017/s0022112056000032.

Lighthill, M. J. (1956b). The image system of a vortex element in a rigid sphere. *Mathematical Proceedings of the Cambridge Philosophical Society*, *52*, 317. doi:10.1017/s0305004100031297.

McLaughlin, J. B. (1993). The lift on a small sphere in wall-bounded linear shear flows. *Journal of Fluid Mechanics*, *246*, 249. doi:10.1017/s0022112093000114.

Miyazaki, K., Bedeaux, D., & Avalos, J. B. (1995). Drag on a sphere in slow shear flow. *Journal of Fluid Mechanics*, *296*, 373. doi:10.1017/s0022112095002163.

Möller, T., & Hughes, J. F. (1999). Efficiently building a matrix to rotate one vector to another. *Journal of Graphics Tools*, *4*, 1–4. doi:10.1080/10867651.1999.10487509.

Ouchene, R., Khalij, M., Arcen, B., & Tanière, A. (2016). A new set of correlations of drag, lift and torque coefficients for non-spherical particles and large reynolds numbers. *Powder Technology*, *303*, 33–43. doi:10.1016/j.powtec.2016.07.067.

Saffman, P. G. (1965). The lift on a small sphere in a slow shear flow. *Journal of Fluid Mechanics*, *22*, 385. doi:10.1017/s0022112065000824.

Saffman, P. G. (1968). The lift on a small sphere in a slow shear flow - corrigendum. *Journal of Fluid Mechanics*, *31*, 624. doi:10.1017/s0022112068999990.

Sanjeevi, S. K., Kuipers, J., & Padding, J. T. (2018). Drag, lift and torque correlations for non-spherical particles from stokes limit to high reynolds numbers. *International Journal of Multiphase Flow*, *106*, 325–337. doi:10.1016/j.ijmultiphaseflow.2018.05.011.

Sommerfeld, M., van Wachem, B., & Oliemans, R. (2008). *ERCOFTAC Best Practice Guidelines: Computational Fluid Dynamics of Dispersed Multi-Phase Flows*. ERCOFTAC.

Stone, H. A. (2000). Philip saffman and viscous flow theory. *Journal of Fluid Mechanics*, *409*, 165–183. doi:10.1017/s0022112099007697.

Tsorng, S., Capart, H., Lo, D., Lai, J., & Young, D. (2008). Behaviour of macroscopic rigid spheres in lid-driven cavity flow. *International Journal of Multiphase Flow*, *34*, 76–101. doi:10.1016/j.ijmultiphaseflow.2007.06.007.

Zastawny, M., Mallouppas, G., Zhao, F., & van Wachem, B. (2012). Derivation of drag and lift force and torque coefficients for non-spherical particles in flows. *International Journal of Multiphase Flow*, *39*, 227–239. doi:10.1016/j.ijmultiphaseflow.2011.09.004.